



# Opto-electronic properties of solution-processed zinc oxide thin films: role of solvents and doping

B. Hanna<sup>1,2</sup> · M. Manuraj<sup>1</sup> · K. P. Surendran<sup>2,3</sup> · K. N. Narayanan Unni<sup>1,2</sup>

Received: 21 February 2020 / Accepted: 29 June 2020 / Published online: 8 July 2020  
© Springer Science+Business Media, LLC, part of Springer Nature 2020

## Abstract

Undoped zinc oxide (ZnO) and nitrogen-doped zinc oxide (NZO) thin films were prepared on transparent conducting oxide-coated glass substrates by employing sol–gel technique. The effect of different solvents and nitrogen doping on the optical, structural, and electrical properties was investigated by UV–visible absorption spectroscopy, atomic force microscopy (AFM), X-ray diffraction (XRD), profilometry, and Hall effect studies. ZnO films yielded transmittance above 85% and the bandgap of ZnO thin films decreased with doping. XRD pattern confirmed hexagonal wurtzite structure of ZnO. NZO thin films were found to be in the nano-thin film phase with thickness of 40 nm. Hall effect studies yielded carrier concentration of  $1.2 \times 10^{15} \text{ cm}^{-3}$  and  $2.03 \times 10^{14} \text{ cm}^{-3}$ , respectively, for undoped and doped ZnO thin films. The changes in vibrational modes of ZnO due to nitrogen doping were detected using Fourier transform infrared (FTIR) analysis. It was found that p-type doping, leading to an improved surface morphology, led to a reduction in optical bandgap and an increased charge carrier mobility. The choice of the solvent was found to have a profound influence on the surface morphology, optical bandgap, tail states distribution, and charge carrier mobility.

## 1 Introduction

Transparent conducting films have a wide range of applications in optoelectronic devices. Low resistivity, high transmittance in the visible range, and high stability against heat are the important and highly desired properties of transparent conducting films [1]. Most of the transparent conducting oxides such as indium tin oxide (ITO), fluorine-doped Tin Oxide (FTO), etc., have high cost, low stability to H<sub>2</sub>

plasma, and toxicity. On the other hand, zinc oxide (ZnO) is a low-cost and comparatively stable material with high transmission [2–4]. ZnO is a wide direct bandgap semiconductor which finds application in thin film transistors [5], light emitting diodes [6], solar cells [7, 8], sensors [9], photodetectors [10], and in photocatalysis [11]. Most of the optoelectronic applications require high carrier mobility and consequently, doping of ZnO becomes essential. ZnO thin films are prepared by various deposition techniques such as sputtering [12], chemical vapor deposition (CVD) [13], pulsed laser deposition (PLD) [14], molecular beam epitaxy (MBE) [15], spray pyrolysis [16], sol–gel process [17–19], etc. Compared to other methods, sol–gel process is a simple, low-cost, and effective method to produce high-quality thin films. In addition, it is easy to control the composition and to fabricate large-area thin films. Although sol–gel process is an easier technique for fabricating thin films, there are certain critical factors influencing the physical, optical and electronic properties of ZnO thin films. These factors include pre-annealing temperature, post-annealing temperature and film thickness. Since ZnO is intrinsically n-type semiconductor, one of the major challenges in the development of ZnO-based optoelectronic devices is to get an efficient p-type ZnO [18]. Recently researchers have been working on p-type ZnO by doping with different elements (N, N–Al,

**Electronic supplementary material** The online version of this article (<https://doi.org/10.1007/s10854-020-03913-7>) contains supplementary material, which is available to authorized users.

✉ K. N. Narayanan Unni  
unni@niist.res.in

<sup>1</sup> Photosciences and Photonics Section, Chemical Sciences and Technology Division, CSIR-National Institute for Interdisciplinary Science and Technology, Thiruvananthapuram, Kerala 695019, India

<sup>2</sup> Academy of Scientific and Innovative Research (AcSIR), Ghaziabad 201002, India

<sup>3</sup> Functional Materials Section, Materials Science and Technology Division, CSIR-National Institute for Interdisciplinary Science and Technology, Thiruvananthapuram, Kerala 695019, India

Li, As, Na, P and K) using various techniques [19–24]. Because of nitrogen's low ionization energy, ionic radius comparable with oxygen, ease of handling, low toxicity, and source-abundance, it can be considered as the most promising dopant [25, 26]. Although solution processing has been established as an effective and simple technique for ZnO thin film fabrication, the very same attractive features need to be maintained while we fabricate p-doped ZnO thin films by solution processing. Precursor solvent is reported to play an important role in defining the opto-electrical properties of spin-coated transparent conducting ZnO:Ga thin films [27]. Similarly, the molar ratio of the precursor is also important. It is important to understand the behavior of the doped film in the nano-thin film regime (less than 50 nm). However, detailed studies on the optoelectronic properties of ZnO nano-thin film prepared by solution processing with special emphasis on the effect of solvents and electrical doping are scarce in literature. In the present work, we have attempted to dope ZnO with nitrogen through a solution processing technique and to study the optical and electrical properties of the doped films, keeping the molar ratio of the precursor material, zinc acetate dihydrate ( $\text{Zn}(\text{CH}_3\text{COO})_2 \cdot 2\text{H}_2\text{O}$ ) constant. Thickness of the film is another critical factor and most of the previous reports deal with thicker ZnO films as given in the electronic supplementary material while we report on the p-type doping effect on a nano-thin film of ZnO, which is having a thickness of 40 nm.

## 2 Experimental

In this work, we prepared both doped and undoped ZnO by sol-gel process and thin films were deposited by spin-coating. Two different 0.5 molar solutions of undoped ZnO were prepared using 2-methoxyethanol and isopropyl alcohol as solvents. In both cases, zinc acetate and monoethanolamine were used as the solute and stabilizing agent, respectively. The solutions were named as ZnO-1 (2-methoxyethanol), ZnO-2 (isopropyl alcohol). ZnO-1 was stirred for 12 h at 60 °C. ZnO-2 was stirred for 2 h at 60 °C and aged at room temperature for 24 h. The solutions were spin-coated on ultrasonically cleaned and subsequently UV-ozone-treated ITO-coated glass substrates at 1500 rpm and the films were annealed at 170 °C for 1 h in air.

N-doped ZnO (NZO) nano-thin films were prepared by adding ammonium acetate as the dopant precursor to ZnO-1. The solution was stirred for 2 h at 60 °C and aged at room temperature for 72 h. The solution was spin coated at 1500 rpm on ultrasonically cleaned and subsequently UV-ozone-treated FTO-coated glass substrates. The samples were annealed at 250 °C for 10 min and the process was repeated for 8 times to get the required thickness. The thin films were post-heated at 500 °C for 1.5 h in the  $\text{N}_2$

atmosphere. In all the three samples, the molar ratio of  $\text{Zn}(\text{CH}_3\text{COO})_2 \cdot 2\text{H}_2\text{O}$  is kept constant at 0.5.

Optical properties of the doped and undoped ZnO thin films were studied by using PerkinElmer UV/VIS/NIR Spectrometer, Lambda 950. Surface morphology of the thin films were investigated by Bruker AFM. Bruker Stylus Profilometer was used for the thickness measurements. X-ray diffraction (XRD) patterns were recorded by XPert-PRO Scan Diffractometer with  $\text{Cu K}\alpha$  ( $\lambda = 1.5406 \text{ \AA}$ ) radiation from 20° to 60° scanning range. Hall effect measurements were done using physical property measurement system (PPMS) from Quantum Design, in a van der Pauw configuration with  $1 \times 1 \text{ cm}^2$  sample size. Fourier transform infrared (FTIR) spectra of doped and undoped thin films were measured by IR Prestige-21 Fourier Transform Infrared Spectrophotometer, Shimadzu.

## 3 Results and discussion

All our measurements have been done at RT. Temperature might not appreciably affect the p-type conductivity because the film is annealed at 500 °C during the film preparation stage. The process conditions have been optimized for a good quality film and we do understand that any variation in the process conditions may have a profound influence on the conductivity of doped ZnO films as previously reported [15, 28, 29].

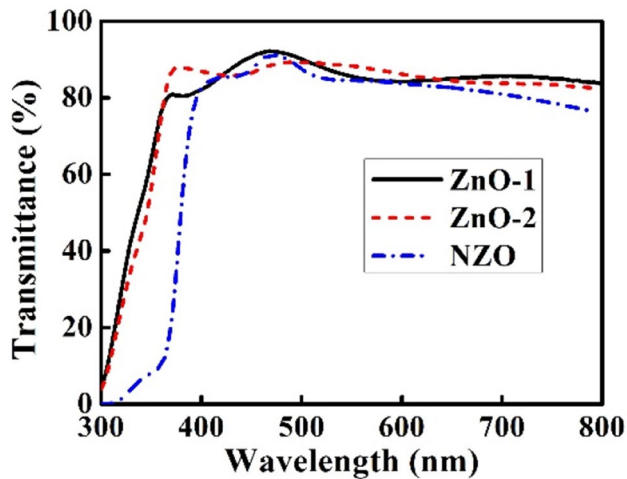
### 3.1 Optical properties

Figure 1 shows the UV-visible transmission spectra of ZnO thin films. ZnO films yielded transmittance above 85%. From the transmittance spectra, it is clear that the UV absorption edge was red shifted upon nitrogen doping. The interference fringes in the transmission spectra are indicative of the high surface quality and homogeneity of the films [30].

The values of the energy bandgap of both doped and undoped ZnO were measured from the Tauc's plot by employing the relation,

$$\alpha h\nu = A(h\nu - E_g)^n, \quad (1)$$

where  $\alpha$  is an absorption coefficient,  $A$  is the proportionality constant,  $h\nu$  is the incident energy, and  $E_g$  is the bandgap of the material [31]. Since ZnO is a direct bandgap semiconductor [32], value of  $n$  is given by 1/2. Figure 2 shows the Tauc's plot of doped and undoped ZnO. The optical bandgap of ZnO-1, ZnO-2, and NZO are summarized in Table 1. The results suggest that the optical bandgap of NZO shows slightly lower value than that of the pure ZnO. The value of energy bandgap of ZnO-2 is smaller than that of ZnO-1. The difference in the bandgap of ZnO thin films in different



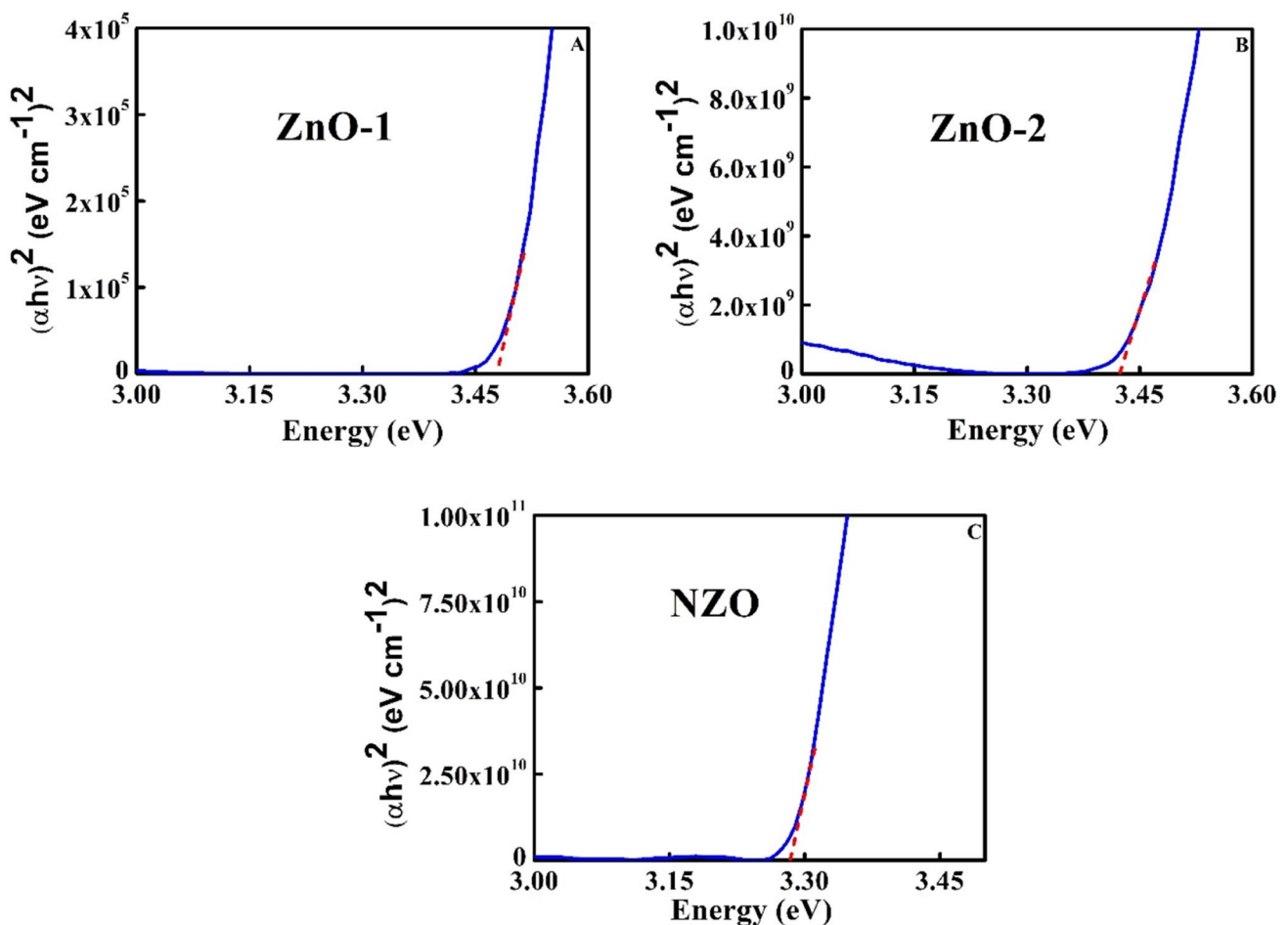
**Fig. 1** UV-visible transmission spectra of doped and undoped ZnO thin films

solvents is due to the dependence of microstructure and morphology of the film on the solvent, which would change the interatomic interactions and thereby the optical properties of the thin films [33].

The relation between absorption coefficient and photon energy near band edge is given by the Urbach relation [34],

$$\alpha = \alpha_0 \exp (hv/E_u), \quad (2)$$

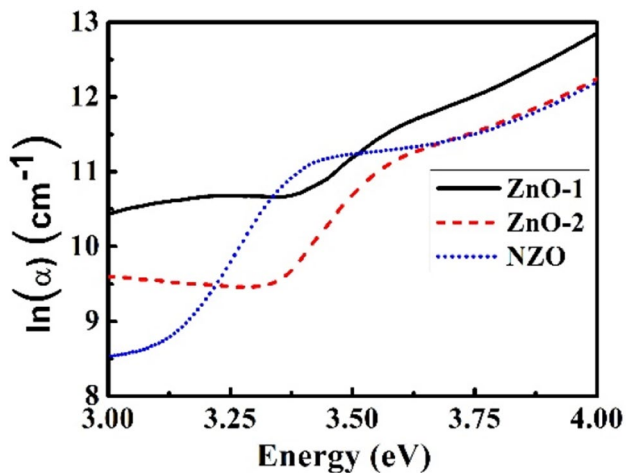
where  $\alpha_0$  is a constant and  $E_u$  is the width of the localized states or Urbach energy. The Urbach energy of the ZnO thin films can be measured from the slope of the graph plotted between  $\ln(\alpha)$  and  $h\nu$ . Figure 3 shows the plot of  $\ln(\alpha)$  vs.  $h\nu$ . The values of Urbach energy of doped and undoped ZnO thin films are given in Table 1. We found that Urbach energy decreases upon doping and that of ZnO-2 is smaller than ZnO-1. This implies that more defect levels are introduced when we use 2-methoxyethanol as solvent. The decrease in the Urbach energy in NZO indicates the decrease in the defect states of thin films.



**Fig. 2** Tauc's plot for a ZnO-1, b ZnO-2, c NZO thin films

**Table 1** Values of optical energy bandgap and Urbach energy of ZnO-1, ZnO-2 and NZO thin films

| Sample | Energy bandgap (eV) | Urbach energy (eV) |
|--------|---------------------|--------------------|
| ZnO-1  | 3.47                | 0.308              |
| ZnO-2  | 3.42                | 0.217              |
| NZO    | 3.29                | 0.129              |

**Fig. 3** Urbach plot of ZnO-1, ZnO-2, and NZO thin films

### 3.2 Morphological and structural properties

AFM images of doped and undoped ZnO thin films obtained by tapping mode are shown in Fig. 4. AFM study reveals that nitrogen doping increases the average grain size and enhances the surface roughness of the thin films. The properties of the ZnO thin film surface, i.e., the surface roughness, grain size, and RMS values are strongly affected by the choice of solvents used for the preparation of ZnO thin films [32, 35]. From the AFM images, it is evident that for ZnO-2, the RMS values are greater than that of ZnO-1. High-quality thin films have been obtained for ZnO-1 and hence we decided to use only ZnO-1 for p-type doping studies. The RMS values of NZO are greater than that of ZnO-1. The RMS values of ZnO-1, ZnO-2, and NZO are given in the Table 2. The grain size of ZnO-2 looks larger probably due to the agglomeration. The thickness of the doped and undoped ZnO thin films was measured by stylus profilometer. The thickness values are 60 nm, 100 nm, and 40 nm for ZnO-1, ZnO-2, and NZO, respectively. The difference in thickness of ZnO-1 and ZnO-2 is due to the difference in the solubility of the precursor materials in the solvents, since molar ratio is fixed in all the cases. To get an appreciable thickness, the spin-coating process was repeated 8 times. It is understood that these process variations might have added to the RMS surface roughness of these films.

The crystal structure analysis of these thin films was done by using XRD. The XRD patterns of ZnO thin films are shown in Fig. 5. For undoped ZnO-1, (002) and (110) peaks were obtained and for ZnO-2, (002), (101), and (110) peaks were observed. For NZO, (100), (002), (101), (102), and (110) peaks were observed. The results are summarized in the Table 3. All the XRD peaks were identified with the standard card JCPDS 36-1451 in the recorded range of  $2\theta$ . It is concluded that the thin films are crystallized in hexagonal wurtzite structure and there was no preferential growth orientation [36].

The crystallite size  $D$  was calculated using Scherrer's relation given in Eq. (3),

$$D = \frac{K\lambda}{\beta \cos \theta}, \quad (3)$$

where  $K$  is a constant,  $\lambda$  is the X-ray wavelength and  $\beta$  is the full width at half maximum (FWHM) [37]. The results suggest that there is a shift in the (002) and (110) planes of ZnO-1 and NZO due to the difference in the ionic radii of O and N. Ionic radii of N is greater than that of O [38]. N substituting O will produce a strain in the crystal and causes shift in XRD peaks to higher or lower angles [38]. The XRD patterns show that both the undoped ZnO thin films prepared with the solvents, 2-methoxyethanol, and isopropyl alcohol exhibit the highest intensity XRD peak on the (002) plane located at  $33.4^\circ$ . However, NZO thin film exhibits the highest intensity XRD peak on the (101) plane located at  $36.632^\circ$ . Therefore, the crystallite size along the plane (002) was calculated for ZnO-1 and ZnO-2 and that of NZO was calculated along (101) plane [31]. The crystallite size of the films is summarized in Table 2. The results show that the crystallite size and thickness of ZnO-1 is smaller than that of ZnO-2 which could be due to the higher viscosity of isopropyl alcohol compared with 2-methoxyethanol. This indicates that 2-methoxyethanol is a better solvent and its fast drying characteristics of ZnO precursor layers, leads to more compact assembly of smaller crystals with less pinholes on annealing. The results are in agreement with findings from the AFM studies. Preferential crystallite orientation can be determined from texture coefficient (TC) and it is given by [39],

$$TC = \frac{\frac{I(hkl)}{I_0(hkl)}}{\frac{1}{N} \sum_n \frac{I(hkl)}{I_0(hkl)}}, \quad (4)$$

where  $I(hkl)$  is the measured intensity of the peak,  $I_0(hkl)$  is the relative intensity of the plane from JCPDS data, and  $N$  is the number of reflections. TC of ZnO-1, ZnO-2, and NZO were calculated. Highest value of TC was obtained for (002) plane in ZnO-1 and ZnO-2. This means that more number of crystallites are oriented along (002) plane. But for NZO,

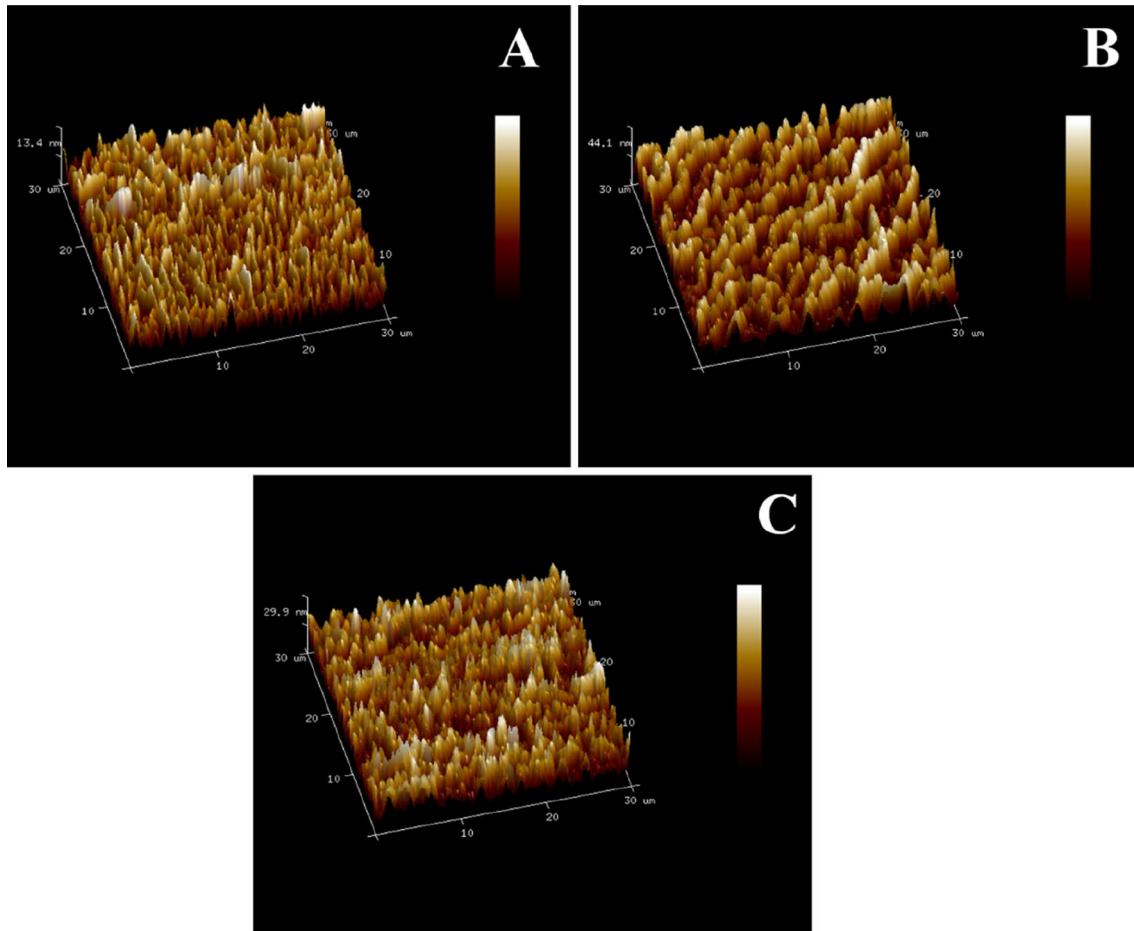


**Fig. 4** AFM images of ZnO thin films. **a** ZnO-1, **b** ZnO-2, **c** NZO

**Table 2** Values of RMS surface roughness and crystallite size of ZnO-1, ZnO-2, and NZO

| Sample | RMS surface roughness (nm) | Crystallite size (nm) |
|--------|----------------------------|-----------------------|
| ZnO-1  | 70.4                       | 15.6                  |
| ZnO-2  | 105                        | 21.8                  |
| NZO    | 81.3                       | 27.6                  |

highest value of  $TC$  was obtained for (110) plane.  $TC$  of (002) plane of NZO film was less than that of the (002) plane of ZnO-1. When doped with nitrogen, the preferential crystallite orientation changes and the crystallites are randomly oriented. This increases the surface roughness of the film. The values of  $I/I_0$  and  $TC$  of all the planes ZnO-1, ZnO-2, and NZO are summarized in Table 3.

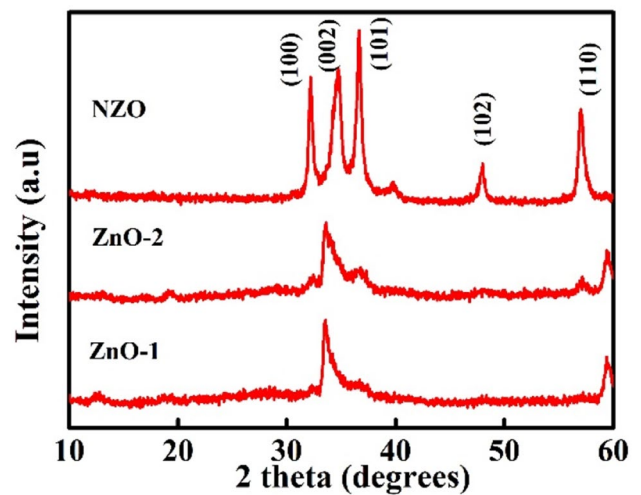


**Fig. 5** XRD pattern of ZnO-1, ZnO-2, and NZO

**Table 3** The structure parameters obtained from XRD studies on ZnO-1, ZnO-2, and NZO

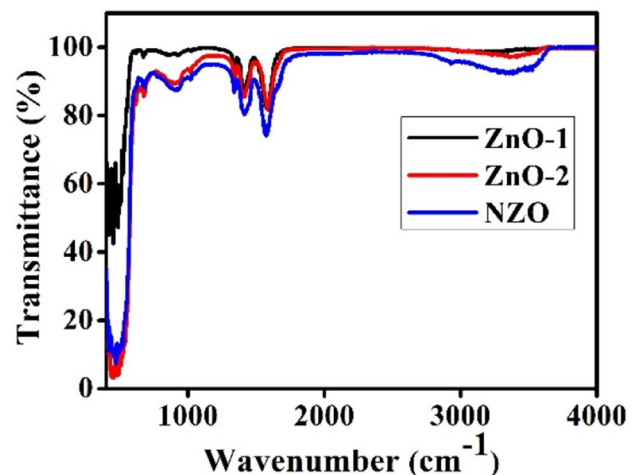
| Sample | Number of peaks | Peak position ( $2\theta$ ) | (hkl) | $d$ spacing ( $\text{\AA}$ ) | FWHM  | $III_0$ | TC    |
|--------|-----------------|-----------------------------|-------|------------------------------|-------|---------|-------|
| ZnO-1  | 1               | 33.444                      | 002   | 2.677                        | 0.554 | 2.272   | 1.07  |
|        | 2               | 59.502                      | 110   | 1.600                        | 0.554 | 1.963   | 0.927 |
| ZnO-2  | 1               | 33.465                      | 002   | 2.675                        | 0.396 | 2.272   | 2.120 |
|        | 2               | 36.759                      | 101   | 2.442                        | 0.950 | 0.214   | 0.200 |
|        | 3               | 57.062                      | 110   | 1.612                        | 0.950 | 0.720   | 0.673 |
| NZO    | 1               | 32.154                      | 100   | 2.781                        | 0.396 | 1.220   | 0.938 |
|        | 2               | 34.729                      | 002   | 2.580                        | 0.356 | 1.713   | 1.310 |
|        | 3               | 36.632                      | 101   | 2.451                        | 0.316 | 1.000   | 0.768 |
|        | 4               | 47.912                      | 102   | 1.897                        | 0.475 | 0.807   | 0.666 |
|        | 5               | 56.914                      | 110   | 1.616                        | 0.277 | 1.763   | 1.350 |

**Table 4** Values of carrier concentration, conductivity, mobility, and carrier type of doped and undoped ZnO thin films

| Sample               | Carrier Concentration ( $n/p$ ) ( $\text{cm}^{-3}$ ) | Conductivity ( $\sigma$ ) (S/cm) | Mobility ( $\mu$ ) ( $\text{cm}^2/\text{Vs}$ ) | Carrier type |
|----------------------|--|----------------------------------|--|--------------|
| ZnO-1 (ITO contact)  | $1.2 \times 10^{15}$                                 | $1.05 \times 10^{-5}$            | 0.05   | n            |
| ZnO-2 (ITO contact)  | $4.84 \times 10^{15}$                                | $6.77 \times 10^{-5}$            | 0.08   | n            |
| NZO (ITO/Pt contact) | $2.03 \times 10^{14}$                                | $7.35 \times 10^{-6}$            | 0.23   | p            |

### 3.3 Electrical properties

The electrical and electronic properties of the thin films were studied by two probe measurement and Hall effect. We calculated the conductivity from two probe measurement and carrier concentration from Hall effect method. The values of conductivity, carrier concentration, carrier type, and mobility of doped and undoped ZnO thin films are listed in Table 4. Inherent n-type conductivity of ZnO-1 and ZnO-2 is due to the native point defects in the ZnO thin films [18]. The interstitial H-atoms form bonds with O and Zn and these act as a shallow donor level and contribute to the n-type conductivity [18]. In NZO, N is substituted for O and this acts as deep acceptor level and contributes to the p-type conductivity [18]. The conductivity of ZnO-1, ZnO-2, and NZO was measured by two probe method by using ITO contacts and that of NZO was found to be one order less. Low conductivity of NZO is due to the high injection barrier for holes when ITO contact is used. Hence Pt contacts were deposited over ITO using PT-1 platinum paste (Dyesol) and we found that the conductivity has increased from  $4.67 \times 10^{-7}$  S/cm (ITO contact) to  $7.35 \times 10^{-6}$  S/cm (ITO/Pt contact). Basically, ZnO is a n-type semiconductor and when doped with N, it passivates all the donor levels and this increases the hole concentration [40]. This is the reason why carrier concentration of NZO (holes) appears to be less than that of ZnO-1 and ZnO-2 (electrons). However, the increased mobility and the change of sign of the majority carrier give evidence to the p-type doping.

**Fig. 6** FTIR spectra of doped and undoped ZnO thin films

### 3.4 FTIR analysis

To understand the presence of molecular species in the doped and undoped samples and to find the effect of doping on the vibrational modes of undoped ZnO, FTIR measurements were done from 400 to 4000/cm at room temperature. FTIR spectra of doped and undoped samples are shown in Fig. 6. Absorption peaks observed below 1000/cm correspond to interatomic vibrations of metal oxides [17]. The absorption bands between 480 and 580/cm are due to Zn–O stretching mode [38]. The peak observed near 900/cm corresponds to the hydrogen substituted at the oxygen site

bound to the lattice Zn site (i.e., Zn–H) [41]. The oxygen replaced by hydrogen may act as a shallow donor level and contributes to the n-type conductivity of undoped ZnO. The absorption bands near 1330/cm, 1400/cm, and 1570/cm were observed for doped and undoped samples and correspond to symmetric and asymmetric stretching vibrations of C=O group [42]. Small variations in the IR peak positions in the region 1000–1500/cm are due to the effect of solvent and N doping. The peak at 2930/cm was observed only for NZO, indicating the presence of N in the NZO [43]. The absorption peak near 3400/cm is due to the O–H stretching mode [44] and it becomes more symmetrical with nitrogen doping.

## 4 Conclusions

We have fabricated doped and undoped ZnO thin films by a relatively facile process through sol–gel technology. P-type doping was done which improved the surface morphology of the film and resulted in a reduction in the value of bandgap. P-doped ZnO was in the nano-thin film form with thickness 40 nm. The thin films were crystalline with crystallite sizes, 15.6 nm, 21.8 nm, and 27.6 nm for ZnO-1, ZnO-2, and NZO, respectively. Mobility values of 0.05 cm<sup>2</sup>/Vs, 0.08 cm<sup>2</sup>/Vs, and 0.23 cm<sup>2</sup>/Vs were obtained for ZnO-1, ZnO-2, and NZO, respectively. The inherent n-type behavior of ZnO-1 and ZnO-2 is due to the H substituted at the O site and that is proved by FTIR measurements. As a p–n junction of ZnO is a pre-requisite for several optoelectronic applications, the results are relevant for flexible and transparent electronics, based on solution-processed ZnO.

**Acknowledgements** One of the authors (HB) acknowledges support from University Grants Commission (UGC) of India and NUKN acknowledge support from DST-AISRF program, Department of Science and Technology, Govt. of India.

## References

1. S. Lany, A. Zunger, *Phys. Rev. Lett.* **98**, 045501 (2007)
2. M. Zhao, F. Shang, J. Lv, Y. Song, F. Wang, Z. Zhou, G. He, M. Zhang, X. Song, Z. Sun, Y. Wei, X. Chen, *Nanoscale Res. Lett.* **9**, 485 (2014)
3. X. Duan, C. Li, L. Fu, Y. Wu, G. Chen, K. Xu, L. Shao, P. Yang, Z. Yu, P. Ding, H. Ma, Y. Li, Y. Du, *Superlattices Microstruct.* **128**, 30 (2019)
4. E.T. Seid, F.B. Dejene, *J. Mater. Sci. Mater. Electron.* **30**, 11833 (2019)
5. S. Thiemann, M. Gruber, I. Lokteva, J. Hirschmann, M. Halik, J. Zaumseil, *A.C.S. Appl. Mater. Interfaces* **5**, 1656 (2013)
6. A. Ghorai, S. Bayan, N. Gogurla, A. Midya, S.K. Ray, *A.C.S. Appl. Mater. Interfaces* **9**, 558 (2017)
7. J. Wei, Z. Yin, S.C. Chen, Q. Zheng, *A.C.S. Appl. Mater. Interfaces* **9**, 6186 (2017)
8. D. Barpuzary, A.S. Patra, J.V. Vaghasiya, B.G. Solanki, S.S. Soni, M. Qureshi, *A.C.S. Appl. Mater. Interfaces* **6**, 12629 (2014)
9. G. Algün, N. Akçay, *J. Mater. Sci.: Mater. Electron.* **30**, 16124 (2019)
10. B. Hanna, K. P. Surendran, K.N. Narayanan Unni, *RSC Adv.* **8**, 37365 (2018)
11. A. Di Mauro, M.E. Fragalà, V. Privitera, G. Impellizzeri, *Mater. Sci. Semicond. Process.* **69**, 44 (2017)
12. A. Barhoumi, L. Yang, N. Sakly, H. Boughzala, G. Leroy, J. Gest, J.-C. Carru, S. Guermazi, *Eur. Phys. J. Appl. Phys.* **62**, 20302 (2013)
13. S.-H. Park, J.-W. Park, S.-M. Yang, K.-H. Kim, N.-M. Hwang, *J. Phys. Chem. C* **119**, 25047 (2015)
14. M. Girtan, M. Kompitsas, R. Mallet, I. Fasaki, *Eur. Phys. J. Appl. Phys.* **51**, 33212 (2010)
15. M. Suja, S.B. Bashar, M.M. Morshed, J. Liu, *A.C.S. Appl. Mater. Interfaces* **7**, 8894 (2015)
16. I. Chaki, A. Belayachi, T. El Bahraoui, M. Regragui, M. Abd-Lefdil, *Eur. Phys. J. Appl. Phys.* **68**, 30301 (2014)
17. M.F. Khan, A.H. Ansari, M. Hameedullah, E. Ahmad, F.M. Husain, Q. Zia, U. Baig, M.R. Zaheer, M.M. Alam, A.M. Khan, Z.A. AlOthman, I. Ahmad, G.M. Ashraf, G. Aliev, *Sci. Rep.* **6**, 27689 (2016)
18. A. Janotti, C. G. Van de Walle, *Rep. Prog. Phys.* **72**, 126501 (2009)
19. M. Dutta, T. Ghosh, D. Basak, *J. Electron. Mater.* **38**, 2335 (2009)
20. M. Hjiri, M.S. Aida, O.M. Lemine, L. El Mir, *Mater. Sci. Semicond. Process.* **89**, 149 (2019)
21. L.-W. Weng, W.-Y. Uen, S.-M. Liao, T.-N. Yang, C.-H. Wu, H.-F. Hong, W.-Y. Ma, C.-C. Shen, *Appl. Surf. Sci.* **277**, 1 (2013)
22. L. Yue, Z. Zhang, Y. Ma, W. Zhang, *J. Nanomater.* **2016**, 1 (2016)
23. B. Panigrahy, D. Bahadur, *RSC Adv.* **2**, 6222 (2012)
24. W. Jun, Y. Yintang, *Mater. Lett.* **62**, 1899 (2008)
25. H. Nian, S.H. Hahn, K.-K. Koo, E.W. Shin, E.J. Kim, *Mater. Lett.* **63**, 2246 (2009)
26. Y.J. Zeng, Z.Z. Ye, W.Z. Xu, B. Liu, Y. Che, L.P. Zhu, B.H. Zhao, *Mater. Lett.* **61**, 41 (2007)
27. A.K. Srivastava, J. Kumar, *Mater. Chem. Phys.* **162**, 436 (2015)
28. U. Chaitra, M.G. Mahesha, D. Kekuda, K.M. Rao, *Appl. Phys. A* **125**, 394 (2019)
29. T.K. Pathak, V. Kumar, L.P. Purohit, *Phys. E Low-Dimensional Syst. Nanostructures* **74**, 551 (2015)
30. J. George, K.S. Joseph, B. Pradeep, T.I. Palson, *Phys. Status Solidi* **106**, 123 (1988)
31. M.K. Jayaraj, A. Antony, M. Ramachandran, *Bull. Mater. Sci.* **25**, 227 (2002)
32. P. Raghu, C. S. Naveen, J. Shailaja, and H. M. Mahesh, in *AIP Conf. Proc.* (2016), p. 020469
33. K.L. Foo, M. Kashif, U. Hashim, W.-W. Liu, *Ceram. Int.* **40**, 753 (2014)
34. F. Urbach, *Phys. Rev.* **92**, 1324 (1953)
35. Q. Liang, F. Qiao, X. Cui, X. Hou, *Mater. Sci. Semicond. Process.* **89**, 154 (2019)
36. S.W. Xue, X.T. Zu, W.L. Zhou, H.X. Deng, X. Xiang, L. Zhang, H. Deng, *J. Alloys Compd.* **448**, 21 (2008)
37. P. Scherrer, *Math.-Phys. Kl* **2**, 98 (1918)
38. R. Kumari, A. Sahai, N. Goswami, *Prog. Nat. Sci. Mater. Int.* **25**, 300 (2015)
39. T. Srinivasulu, K. Saritha, K.T.R. Reddy, *Mod. Electron. Mater.* **3**, 76 (2017)
40. D.P. Norton, Y.W. Heo, M.P. Ivill, K. Ip, S.J. Pearton, M.F. Chisholm, T. Steiner, *Mater. Today* **7**, 34 (2004)
41. K. Senthilkumar, M. Tokunaga, H. Okamoto, O. Senthilkumar, Y. Fujita, *Appl. Phys. Lett.* **97**, 091907 (2010)
42. F.S. Ghoreishi, V. Ahmadi, M. Samadpour, *J. Nanostruct.* **3**, 453 (2014)

43. B.M. Keyes, L.M. Gedvilas, X. Li, T.J. Coutts, J. Cryst. Growth **281**, 297 (2005)
44. M.N. Kamalasanan, S. Chandra, Thin Solid Films **288**, 112 (1996)

**Publisher's Note** Springer Nature remains neutral with regard to jurisdictional claims in published maps and institutional affiliations.